

Comparison of two methods for one-dimensional Ga₂O₃-ZnGa₂O₄ core-shell heterostructure synthesis

Edgars Butanovs^{1,*}, Martins Zubkins¹, Ramunas Nedzinskas¹, Veronika Zadin², Boris Polyakov¹

¹Institute of Solid State Physics, University of Latvia, Kengaraga street 8, Riga, Latvia, LV-1063

²Institute of Technology, University of Tartu, Nooruse 1, 50411, Tartu, Estonia

*e-mail: edgars.butanovs@cfi.lu.lv

Abstract

While gallium oxide Ga₂O₃ has recently shown promise as a new ultra-wide bandgap semiconductor in the form of thin films and nanowires (NWs), its widespread applicability is limited due to lack of native p-type conductivity, thus requiring fabrication of heterojunctions. A potential matching material is spinel zinc gallate ZnGa₂O₄. In this work we demonstrated and compared two novel approaches of one-dimensional Ga₂O₃-ZnGa₂O₄ core-shell NW heterostructure preparation: (a) a direct deposition of a ZnGa₂O₄ coating using a reactive magnetron co-sputtering; (b) annealing of a sacrificial few-nm-thick ZnO coating, deposited via atomic layer deposition, at high temperature to enable solid state reaction between ZnO and Ga₂O₃. The as-grown nanostructures were characterized via scanning and transmission electron microscopies, X-ray diffraction and X-ray photoelectron spectroscopy. Room temperature optical features were disclosed using photoluminescence and optical absorption. While both methods are viable for production of the heterostructures, smoother and more uniform ZnGa₂O₄ coating around Ga₂O₃ NWs was obtained via sacrificial layer conversion in comparison to the sputter-deposited one. These heterostructures could potentially be used for photocatalysis and nanoscale ultra-wide bandgap electronics.

Keywords: *A1. Characterization; A3. Chemical vapor deposition processes; A3. Physical vapor deposition processes; B1. Gallium compounds; B1. Oxides; B2. Semiconducting materials.*

1. Introduction

Nanowires (NW) are one-dimensional nanostructures, which exhibit promising properties and new functionalities due to their large surface-to-volume ratio [1,2]. During the last two decades NWs have been extensively studied for applications in next-generation nanoscale electronic and photonic devices [2,3], sensors [4,5], energy storage and conversion [6–8]. Through further modification of their surface one can enhance or tune the nanostructure properties for the desired application, as well as NW surface can exhibit smaller lattice mismatch constraint for heterostructure preparation in comparison to thin films growth [9–13]. Such radial 1D-1D *core-shell* NW heterostructures can be used in efficient electronic and optoelectronic devices [11,14,15].

Gallium oxide (Ga_2O_3) has recently shown promise as a new ultra-wide bandgap (around 4.9 eV) semiconductor [16,17], thus the material has been mainly studied for applications in power electronics [18,19] and ultraviolet (UV) optoelectronics [20]. Alongside thin films, potential of Ga_2O_3 has also been demonstrated in form of NWs for solar-blind deep-UV photodetection [21–23], electronics [24] and sensing [25,26]. One of the main limiting factors for more ubiquitous use of Ga_2O_3 in electronics is the lack of p-type conductivity in the material [27]. While n-type conductivity is easily obtainable by doping with Si or Sn [27,28], p-type conductivity in Ga_2O_3 is practically unattainable due to deep acceptor levels, relatively high effective masses of holes and formation of trapping centres [29]. Therefore, the lack of a native p-type conductivity promotes the search for a matching material for heterojunction fabrication [30,31].

Spinel zinc gallate (ZnGa_2O_4) has recently emerged as a potential bipolar material for ultra-wide bandgap electronics [32,33]. It has 4.6 – 5.2 eV wide bandgap, p-type conductivity, high chemical and thermal stability, hence the promising applicability in power electronics and elsewhere [34–36]. Spinels obey different doping rules (‘self-doping’) from traditional binary

semiconductor oxides because of their multivalent elements and various possible sites, such as the antisite defects, due to the inverted distribution of cations; therefore, making n- and p-type conductivity possible. An acceptor level can be achieved by promoting antisites (Zn_{Ga}) defects, while high donor concentration can be obtained due to the hybridization of the Zn-O orbitals in material grown in Zn-rich conditions [33]. ZnGa_2O_4 has been studied not only in the form of thin films but NWs as well [37,38]. It can be epitaxially grown on $\beta\text{-Ga}_2\text{O}_3$ [39], and this heterostructure have been demonstrated in efficient photocatalysis due to its favourable type-II band alignment [40,41]. Despite the promise in heterojunction fabrication for electronics and photocatalysis applications, this material combination has been little studied.

In this work we demonstrated and compared two novel approaches of one-dimensional $\text{Ga}_2\text{O}_3\text{-ZnGa}_2\text{O}_4$ core-shell NW heterostructure preparation: (a) a direct deposition of a ZnGa_2O_4 coating using a reactive magnetron co-sputtering of zinc and gallium targets in oxygen background gas; (b) annealing of a sacrificial few-nm-thick ZnO coating, deposited via atomic layer deposition (ALD), at high temperature to enable solid state reaction between ZnO and Ga_2O_3 . Such heterostructures could potentially be used for photocatalysis and nanoscale ultra-wide bandgap electronics.

2. Experimental details

Pure Ga_2O_3 NWs were synthesized via atmospheric pressure chemical vapour transport method in a horizontal quartz tube reactor using *vapour-liquid-solid* mechanism and gold nanoparticles as a catalyst. The procedure and characterization of the as-grown NWs has been reported in our previous work [31]. The ZnGa_2O_4 shell was grown around the Ga_2O_3 NWs using two different approaches: (a) direct deposition of a ZnGa_2O_4 coating using a reactive magnetron co-sputtering of zinc and gallium targets in oxygen background gas; (b) annealing

of a pre-deposited few-nm-thick ZnO coating at high temperature to enable solid state reaction between ZnO and Ga₂O₃ [39,42].

A 50 nm thick ZnGa₂O₄ film was deposited on Ga₂O₃ NWs at 600°C by reactive direct current (DC) magnetron co-sputtering from metallic Zn (American Elements, 99.95%) and Ga (PI-KEM, 99.999%) targets in an Ar(99.9999%)/O₂(99.999%) atmosphere. The deposition was performed using a G500M.2 PVD coater (Sidrabe Vacuum, Ltd.) equipped with planar balanced magnetrons (150 mm × 75 mm). The Ga target was in a liquid state during sputtering and placed under the substrate holder parallel to the ground at a distance of 11 cm. The Zn target was placed next to the Ga target and turned towards the substrate. The base pressure was $\leq 7 \times 10^{-4}$ Pa in a turbomolecular pumped chamber. The sputtering pressure was set to 0.50 Pa by feeding 30 sccm (standard cubic centimetres per minute) of Ar, 11 sccm of O₂, and partly closing the throttle valve between the chamber and the pump. Simultaneous sputtering of both targets in DC mode was carried out by a two-channel power supply (Melec, SIP2000USB-10-500-D). The Ga target was sputtered at a constant power of 100 W. Control of the sputtering process was achieved by optical emission spectroscopy (OES), i.e., the sputtering power of Zn was controlled by keeping the ratio $I_{\text{Ga}}/I_{\text{Zn}}$ constant at 2.5, where I_{Ga} and I_{Zn} are the intensities of the excited Ga (417 nm) and Zn (481 nm) emission lines, respectively. In the particular case, the average Zn sputtering power was 145 W. X-ray diffraction (XRD) pattern, scanning electron microscope (SEM) surface image, and UV-Vis-NIR spectroscopy measurements of a 290 nm thick film on a fused quartz deposited at the same conditions is shown in *Fig. S1* for reference.

Amorphous ZnO coating was deposited on the Ga₂O₃ NWs using atomic layer deposition (ALD, Veeco, Savannah S100). 90 cycles of H₂O and diethylzinc (DEZn) injection pulses at 150°C temperature led to growth of a 15 nm thick film. Afterwards, the as-prepared Ga₂O₃-ZnO core-shell NWs were annealed in air for 20 minutes at various temperatures. 850°C

was found to be the optimal temperature for obtaining few-nm thick ZnGa₂O₄ shell. All the results below are given for the sample prepared at these parameters unless noted otherwise.

As-grown core-shell NW morphology was characterized using a SEM (Lyra, Tescan) together with energy-dispersive X-ray spectroscopy (EDX) elemental mapping. The NW crystalline structure was studied using a transmission electron microscope (TEM, Tecnai GF20, FEI) operated at a 200 kV accelerating voltage. The phase composition was determined by XRD using Rigaku MiniFlex 600 X-ray powder diffractometer with Bragg-Brentano θ -2 θ geometry and 600W Cu anode (Cu K α radiation, $\lambda = 1.5406 \text{ \AA}$) X-ray tube. The chemical composition of the NW samples was confirmed with X-ray photoelectron spectroscopy (XPS) measurements performed using an X-ray photoelectron spectrometer ESCALAB Xi (ThermoFisher). Al K α X-ray tube with the energy of 1486 eV was used as an excitation source, the size of the analysed sample area was 650 μm x 100 μm and the angle between the analyser and the sample surface was 90°. An electron gun was used to perform charge compensation. The base pressure during the spectra acquisition was better than 10⁻⁵ Pa.

The room-temperature photoluminescence (PL) measurements were recorded using a custom-made setup. PL was excited using a pulsed solid-state 266 nm laser (4-th harmonic Nd:YAG; > 0.5 μJ). The laser beam was unfocused to avoid damaging the sample. The power density was controlled between 90-650 kW/cm² with fused-silica gradient filter. PL was dispersed by using the 500 mm focal length monochromator (Andor SR-500i; UV-VIS gratings: 1200 g/mm blazing at 300 nm; 600 g/mm blazing at 1000 nm) and focused into photomultiplier tube (PMT) (ACC-SR-ASM-0047; Oxford instruments). The conventional lock-in detection system (SR830; Stanford Research Systems) was used to extract the emission signal. Further experimental details can be found in ref. [43]. Diffusive reflectance spectra were measured in the Shimadzu UV-3600 two beam spectrometer, equipped with a multi-purpose compartment MPC-3100 by means of an integrating sphere (of the 60 mm diameter) coated by

barium sulphate. All spectra were measured relatively in respect of UV-Enhanced aluminium (Al) mirror and corrected by a known absolute reflectance spectrum of the mirror.

3. Results and discussion

The morphology of the as-grown NWs was studied using SEM. Pure Ga_2O_3 NWs (see *Fig.1(a)*) were typically straight, exhibited smooth surface and uniform diameter along their length. When ZnGa_2O_4 film was deposited on top of the NWs via reactive magnetron sputtering (see *Fig.1(c)*), the NW surface roughness visibly increased, as well as some curvature appeared for a large portion of NWs possibly due to non-uniform deposition of the film leading to epitaxial strain bending. On the other hand, when ZnGa_2O_4 coating was obtained on the Ga_2O_3 NWs via conversion of a pre-deposited ZnO ALD coating, the NWs still appeared smooth, straight and with a uniform diameter (see *Fig.1(e)*). EDX mapping was performed in SEM in order to confirm the homogenous distribution of the chemical elements along the length of the as-prepared NWs (*Fig.1(b,d,f)*). In the both core-shell NW cases, Zn was present all along the

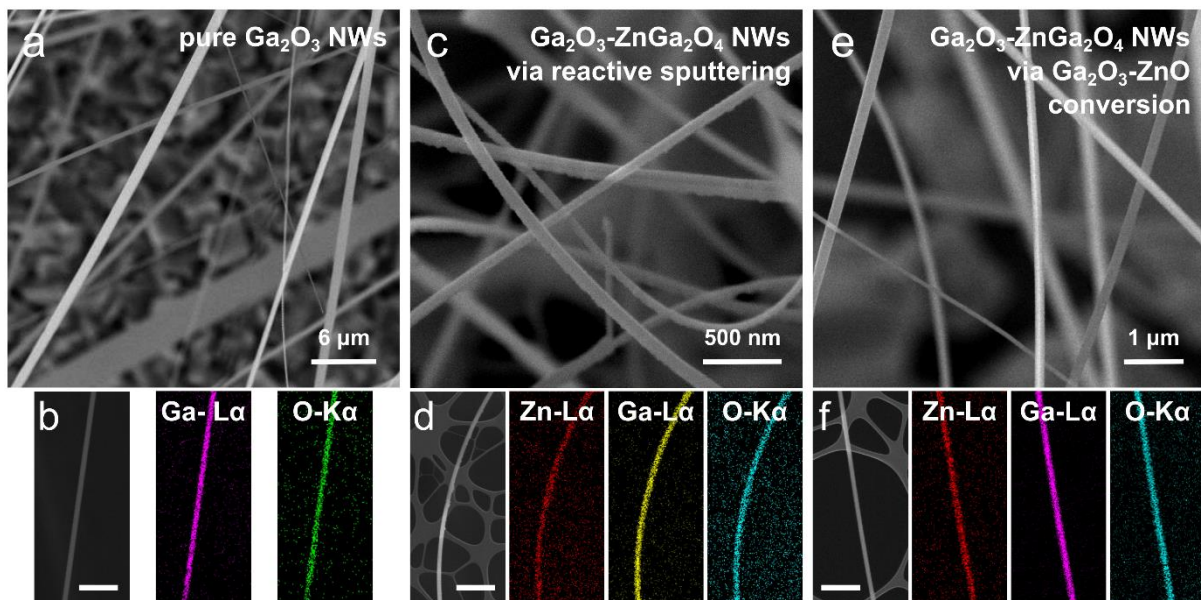


Figure 1. SEM images and EDX elemental mapping of (a,b) pure Ga_2O_3 NWs, $\text{Ga}_2\text{O}_3\text{-ZnGa}_2\text{O}_4$ core-shell NWs prepared via (c,d) reactive magnetron sputtering and (e,f) conversion of a pre-deposited ZnO ALD coating. The EDX mapping shows the uniform distribution of the ZnGa_2O_4 shell along the nanowire; the scalebar corresponds to 2 μm .

NW axis, indicating uniform ZnGa_2O_4 shell growth. The same was observed for Ga and O, however, the main contribution of the signal here most probably is from the Ga_2O_3 core.

High-resolution TEM was used to reveal the inner structure of the core-shell NWs. The core and the few-nanometre shell can be distinguished in the lower magnification images (see *Fig.2(a,c)*) due to the contrast difference. In the case of the NWs prepared via Ga_2O_3 -ZnO conversion the thin shell was uniformly grown around the NW, while the sputter-deposited ZnGa_2O_4 coating typically had a significant thickness difference between the opposite sides of NWs. Since ALD is not a line-of-sight method, the sacrificial ZnO atomic layers were initially deposited homogeneously across the whole NW array, therefore a uniform ZnGa_2O_4 coating forms after the high-temperature annealing. Around 4 nm thick ZnGa_2O_4 shell was obtained from a 15 nm thick ZnO coating, which indicates probable ZnO evaporation alongside the

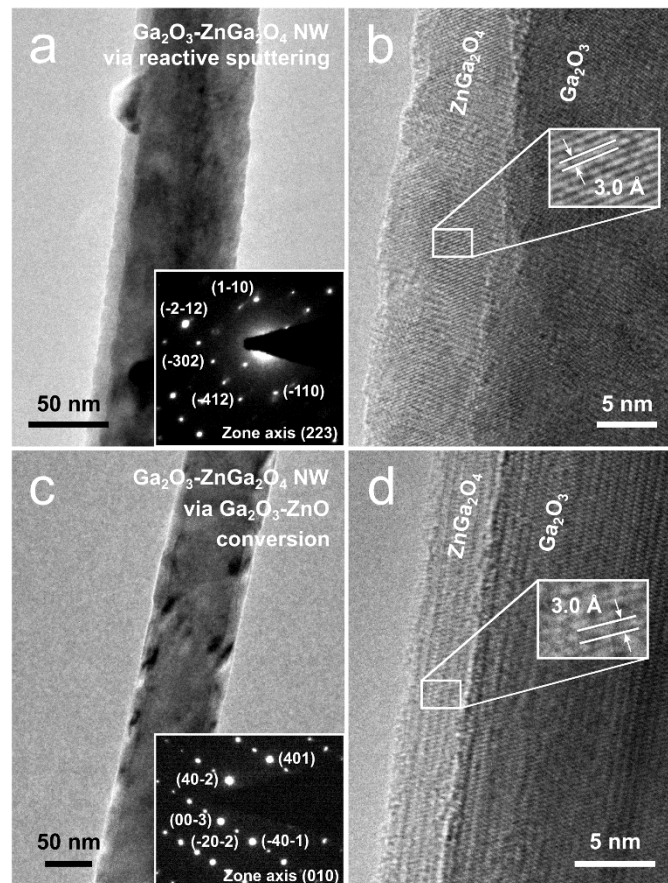


Figure 2. TEM images at different magnifications and corresponding SAED patterns of Ga_2O_3 - ZnGa_2O_4 core-shell NWs prepared via (a,b) reactive magnetron sputtering and (c,d) conversion of a pre-deposited ZnO ALD coating; the insets show the measured d-spacings.

diffusion into the Ga₂O₃ core and the subsequent solid-state reaction. On the other hand, magnetron sputtering is generally considered as a line-of-sight deposition method, therefore, the “shadow” effect leads to a thickness non-uniformity of the coating on the variously oriented NWs. Selected-area electron diffraction (SAED) analysis confirmed the monoclinic phase of Ga₂O₃ core; however, no diffraction signal was obtained from the few-nm thick shell. The crystalline structure of the core-shell NWs can be seen in the higher magnification images (see *Fig.2(b,d)*). For both preparation methods, the interplanar distance values (d-spacings) in the shell were measured to be around 2.9-3.0 Å, which matches well the interatomic distances for (220) planes seen in (111) projection of spinel ZnGa₂O₄ crystal (ICDD-PDF #38-1240; see *Fig.S2* in Supporting information file) [38]. Similarly, the interplanar distance values for the core was also measured to be around 2.8-2.9 Å [44,45], being in a good agreement with the monoclinic Ga₂O₃ phase (ICDD-PDF #41-1103).

The presence of the respective crystalline phases in the NW arrays on Si(100)/SiO₂ substrates was confirmed using XRD measurements (see *Fig.3(a)*). All the patterns contained Bragg peaks from the monoclinic Ga₂O₃ NWs (ICDD-PDF #41-1103). Relatively weaker Bragg peaks of spinel ZnGa₂O₄ phase (ICDD-PDF #38-1240) can be identified in both core-shell NW samples despite the small thickness (few nm) of the coating. Bragg peak at around 33° was attributed to the Si (100) substrate (forbidden Si (200) reflection). XRD patterns for core-shell NWs prepared via conversion of a pre-deposited 15 nm thick ZnO at different temperatures are shown in *Fig.3(b)*. 850°C was found to be the optimal temperature for obtaining few-nm thick ZnGa₂O₄ shell, while lower temperature did not enable the solid-state reaction between Ga₂O₃ and ZnO, and a higher temperature led to an extensive evaporation of the ZnO film. The evolution of the phase composition for core-shell NWs with different sacrificial ZnO coating thicknesses can be seen in *Fig.3(c)*. No detectable spinel ZnGa₂O₄ phase was observed for 5 nm thick sacrificial coating, while the optimal thickness for a few-

nm thick ZnGa₂O₄ shell formation was found to be 15 nm. Thicker ZnO coatings (e.g., 30 nm) led to a significant XRD signal reduction for Ga₂O₃ and increase for ZnGa₂O₄ phases, respectively, a drastically increased NW surface roughness due to a formation of large ZnGa₂O₄ crystallites (see TEM images in Fig.S3 in Supporting information file), and emergence of a small amount of left-over crystalline ZnO.

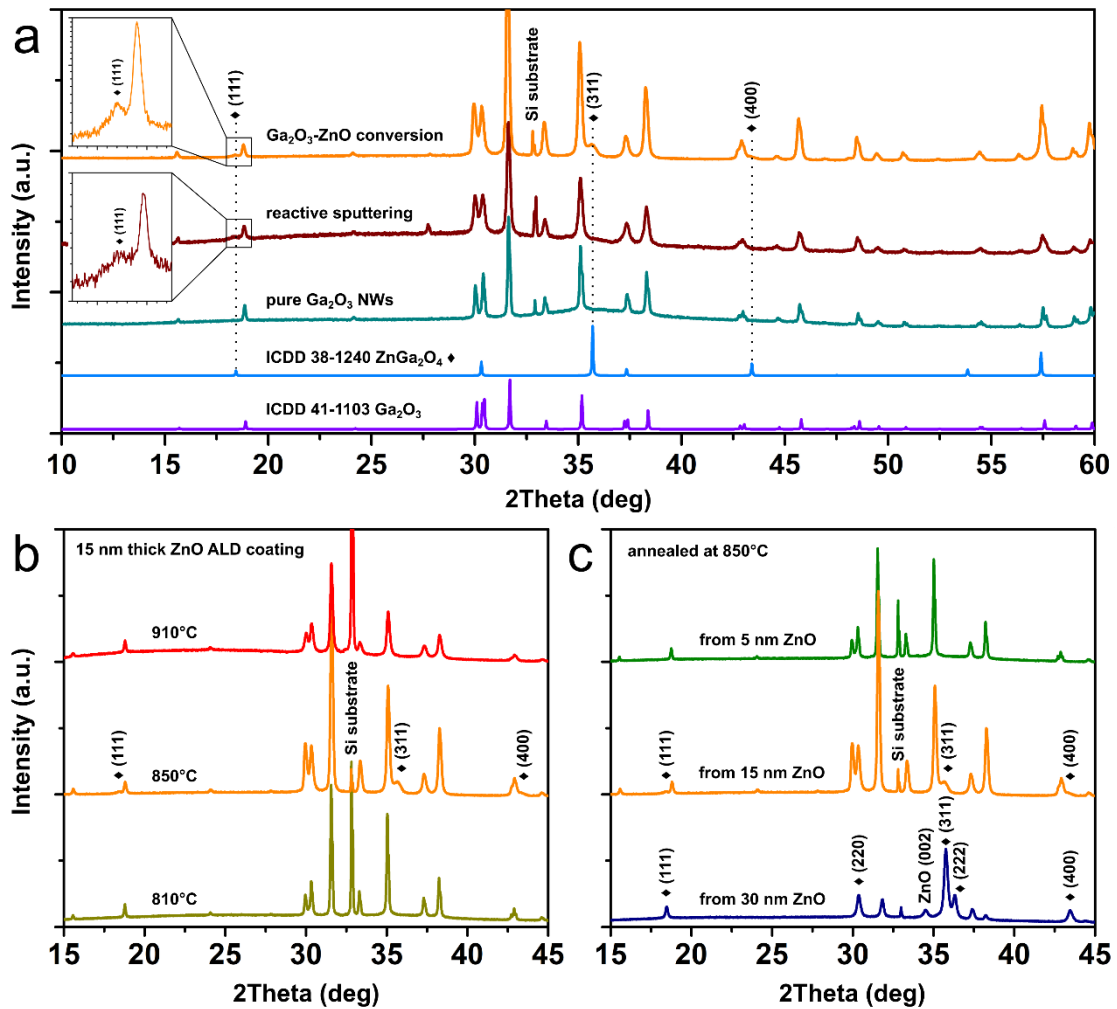


Figure 3. (a) X-ray diffraction (XRD) patterns of pure Ga₂O₃ NW and Ga₂O₃-ZnGa₂O₄ *core-shell* NW arrays on Si(100)/SiO₂ substrates prepared via reactive magnetron sputtering and conversion of a pre-deposited ZnO ALD coating. Spinel ZnGa₂O₄ (111) peaks at 18.4 deg are shown in insets for better clarity. The respective ICDD patterns for each phase are provided for reference. XRD patterns of Ga₂O₃-ZnGa₂O₄ *core-shell* NW arrays prepared via conversion of a pre-deposited ZnO ALD coating (b) at different annealing temperatures (15 nm thick sacrificial ZnO coating) and (c) different ZnO sacrificial coating thickness (annealed at 850°C). The orange XRD pattern in (a-c) is for the same sample prepared at 850°C from a 15 nm thick ZnO coating.

An XPS analysis was performed in order to verify the chemical composition of the prepared Ga₂O₃-ZnGa₂O₄ NWs. High-resolution spectra of Zn 2p, Ga 3d and O 1s were acquired and calibrated relative to adventitious C 1s peak at 285 eV binding energy. Qualitatively similar results were acquired for both synthesis methods (see Fig.4). Zn 2p_{3/2} peak was located at 1022.0 eV (spin-orbit splitting $\Delta_{3/2-1/2} = 23$ eV), Ga 3d peak at 20.0 eV, and O 1s at 530.4 eV, which matches the binding energies of constituent elements in ZnGa₂O₄ compound [33,46]. Worth noting that O 1s peak also contains a contribution at around 532–533 eV from organic surface contaminants (C-O chemical state) and can be seen as a minor shoulder. No significant chemical shift was observed in comparison to pure Ga₂O₃ NWs and ZnO-coated Ga₂O₃ NWs (see Fig.S4 in Supporting information file).

The optical properties of Ga₂O₃-ZnGa₂O₄ core-shell NWs prepared via conversion of a pre-deposited ZnO ALD coating were investigated and compared to pure Ga₂O₃ NWs. The complex optical characterization approach, including the emission- and absorption-type optical

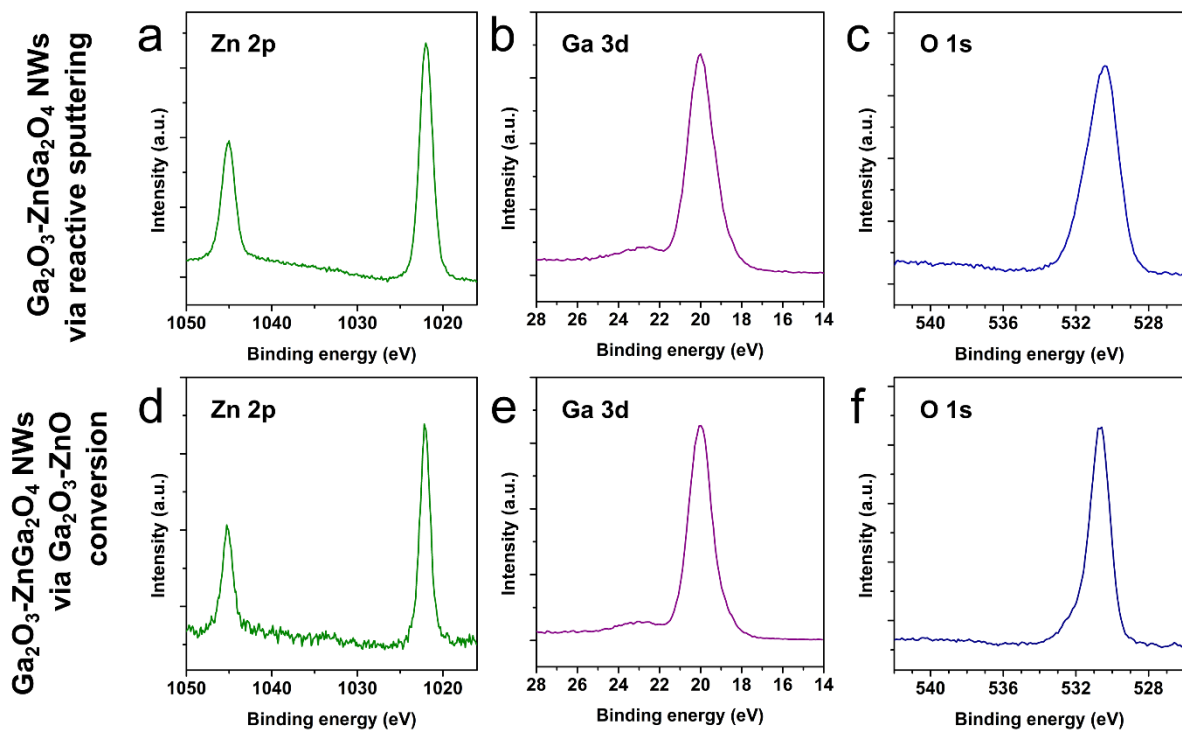


Figure 4. XPS spectra of Ga₂O₃-ZnGa₂O₄ core-shell NW arrays on Si(100)/SiO₂ substrates prepared via (a-c) reactive magnetron sputtering and (d-f) conversion of a pre-deposited ZnO ALD coating, showing the peak scans of the detected elements.

spectroscopy allows obtaining the important Stokes shift energy parameter E_S . By comparing the photoluminescence (see *Fig.5(a)*) and optical absorption (see *Fig.5(b)*) data, the Stokes shift energy of $E_S > 1.1$ eV is established, considering the very start of the absorption onset. A simple analysis suggests that such a high E_S value should indicate the abundance of deep-defect states in the studied NW samples, with the dominant defect-related optical transitions in the emission spectra. Indeed, UV and blue luminescence are closely related to the concentration of O^{-2} vacancies, also the role of surface states in NW structures cannot be neglected. Room temperature normalized PL spectra for pure Ga_2O_3 and Ga_2O_3 - $ZnGa_2O_4$ *core-shell* NWs is shown in *Fig. 5(a)*. Evidently, the high energy PL features of pure Ga_2O_3 and Ga_2O_3 - $ZnGa_2O_4$ NWs match around 3.4 eV. It has been established that PL feature at 3.444 eV (360 nm) should be attributed to self-trapped excitons [47]. However, at lower energies the asymmetric PL shape of pure Ga_2O_3 sample indicate a broad blue-band centred at 3.016 eV (411 nm), as deduced from Gaussian decomposition of PL spectrum (see *Fig.S5(a)*). The latter PL feature is associated with the recombination of a trapped electron in a donor with a trapped hole in an acceptor [47]. While for the Ga_2O_3 - $ZnGa_2O_4$ *core-shell* NWs sample a prominent low energy PL feature was established at 2.806 eV (442 nm; *Fig.S5(b)*), which is related to the self-activation centre of the octahedral Ga-O group in the spinel $ZnGa_2O_4$ -shell lattices [48,49]. The diffuse reflectance R_∞ was measured using an integrating sphere. Absorption spectra was analysed using the Kubelka-Munk approach, taking into account the pseudo-absorption function and considering absorption coefficient under sigmoid-Boltzmann approach [50,51]. The technical details on the method are given in Supporting information file. Experimentally-derived Kubelka-Munk absorption α_{K-M} spectra for the pure Ga_2O_3 NWs along with Ga_2O_3 - $ZnGa_2O_4$ NWs are shown as symbols in *Fig.5(b)*, and sigmoid-Boltzmann function fit, giving reasonable results of the bandgap energy, shown as solid grey lines. For pure Ga_2O_3 NW sample the estimated $E_g = 4.821$ eV show good agreement with the established direct energy

bandgap value for β -Ga₂O₃ ($E_g = 4.9$ eV). Whilst for Ga₂O₃-ZnGa₂O₄ core-shell NW sample, the absorption onset of $\alpha(E)$ spectrum is clearly composed of two different slopes (see Fig. 5(b)), owing to the absorption in Ga₂O₃ ($E_g = 4.674$ eV) and ZnGa₂O₄ ($E_g = 5.013$ eV) parts of the NWs - ensemble, respectively.

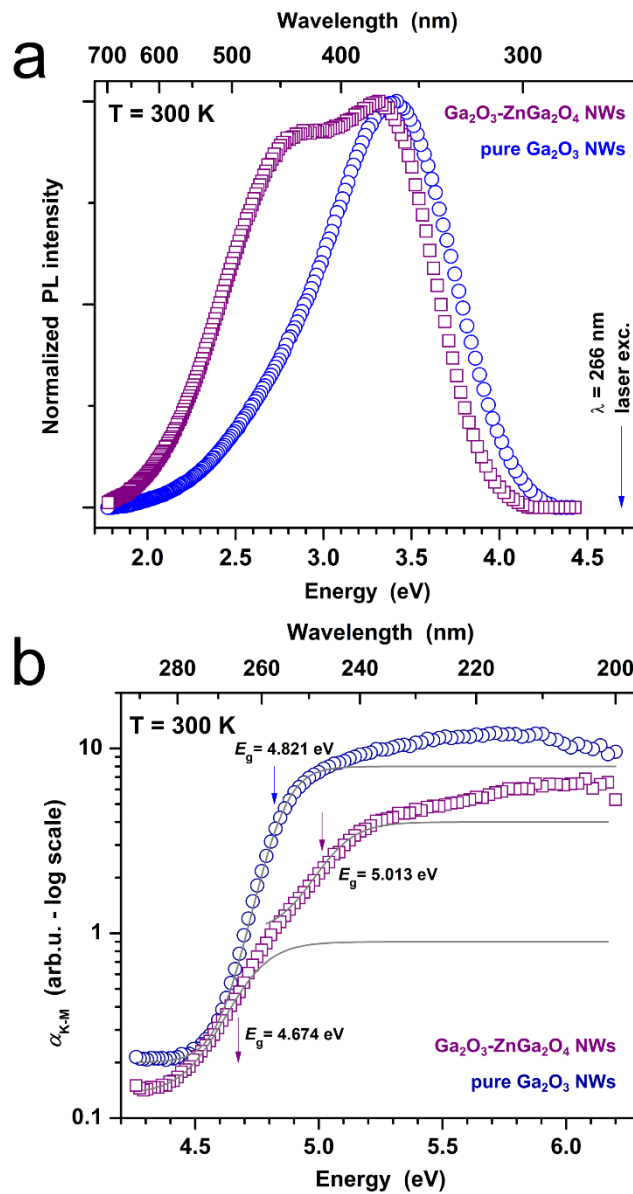


Figure 5. Room temperature normalized (a) PL and (b) absorption spectra of pure Ga₂O₃ and Ga₂O₃-ZnGa₂O₄ core-shell NWs. Energy bandgap E_g values were calculated using the sigmoid-Boltzmann function approach (note the logarithmic scale of absorption spectra).

5. Conclusions

Two novel approaches of one-dimensional Ga₂O₃-ZnGa₂O₄ core-shell NW heterostructure preparation have been demonstrated: (a) a direct deposition of a ZnGa₂O₄ coating using a reactive magnetron co-sputtering of zinc and gallium targets in oxygen background gas; (b) annealing of a sacrificial few-nm-thick ALD ZnO coating to enable solid state reaction between ZnO and Ga₂O₃. 850°C was found to be the optimal annealing temperature for obtaining ZnGa₂O₄ shell, whilst a lower temperature did not enable the solid-state reaction between Ga₂O₃ and ZnO, and a higher temperature led to evaporation of the ZnO film. The as-grown nanostructures were characterized by SEM-EDX, TEM, XRD and XPS. Structural findings were corroborated with room temperature PL and optical absorption spectroscopy, establishing the optical bandgap values and emission features associated with Ga₂O₃ and ZnGa₂O₄. While both methods are viable for production of such heterostructures, smoother and more uniform ZnGa₂O₄ coating around Ga₂O₃ NWs was obtained via conversion of a pre-deposited ZnO ALD layer in comparison to the sputter-deposited one, if the sacrificial layer thickness is selected in the optimal range. Such one-dimensional Ga₂O₃-ZnGa₂O₄ core-shell heterostructures could potentially be used for photocatalysis and nanoscale ultra-wide bandgap electronics.

Acknowledgements

This research was funded by ERDF project No. 1.1.1.1/20/A/057 “Functional ultrawide bandgap gallium oxide and zinc gallate thin films and novel deposition technologies”. V.Z. was supported by the European Union's Horizon 2020 program, under Grant Agreement No. 856705 (ERA Chair “MATTER”). Optical measurements by R.N. were supported from post-doctoral research project 1.1.1.2/VIAA/3/19/442. Institute of Solid State Physics, University of Latvia as the Center of Excellence has received funding from the European Union's Horizon

2020 Framework Programme H2020-WIDESPREAD-01-2016-2017-TeamingPhase2 under grant agreement No. 739508, project CAMART². The authors are grateful to Valts Minders for assistance with materials synthesis.

CRedit author statement

Edgars Butanovs: Conceptualization, Methodology, Investigation, Validation, Visualization, Writing - Original Draft, Writing - Review & Editing, Supervision. **Martins Zubkins:** Investigation, Visualization, Writing - Original Draft. **Ramunas Nedzinskas:** Investigation, Visualization, Writing - Review & Editing. **Veronika Zadin:** Writing - Review & Editing. **Boris Polyakov:** Conceptualization, Investigation, Methodology, Validation, Writing - Review & Editing.

Supporting information

Supporting information is available and contains characterization data for a sputter-deposited ZnGa₂O₄ thin film reference sample, TEM images of Ga₂O₃-ZnGa₂O₄ core-shell NWs prepared via conversion of a pre-deposited 30 nm thick ZnO ALD coating, XPS spectra for pure Ga₂O₃ NWs and Ga₂O₃-ZnO *core-shell* NWs, and additional details on optical characterization.

References

- [1] Dasgupta, N. P. *et al.* 25th Anniversary Article: Semiconductor Nanowires - Synthesis, Characterization, and Applications. *Adv. Mater.* **26**, 2137–2184 (2014)
- [2] Jia, C., Lin, Z., Huang, Y. & Duan, X. Nanowire Electronics: From Nanoscale to Macroscale. *Chem. Rev.* **119**, 9074–9135 (2019)
- [3] Quan, L. N., Kang, J., Ning, C. Z. & Yang, P. Nanowires for Photonics. *Chem. Rev.* **119**, 9153–9169 (2019)

- [4] Fennell, J. F. *et al.* Nanowire Chemical/Biological Sensors: Status and a Roadmap for the Future. *Angew. Chemie Int. Ed.* **55**, 1266–1281 (2016)
- [5] Chen, X., Wong, C. K. Y., Yuan, C. A. & Zhang, G. Nanowire-based gas sensors. *Sensors Actuators B Chem.* **177**, 178–195 (2013)
- [6] Mai, L., Tian, X., Xu, X., Chang, L. & Xu, L. Nanowire Electrodes for Electrochemical Energy Storage Devices. *Chem. Rev.* **114**, 11828–11862 (2014)
- [7] Nehra, M. *et al.* 1D semiconductor nanowires for energy conversion, harvesting and storage applications. *Nano Energy* **76**, 104991 (2020)
- [8] Polyakov, B. *et al.* A comparative study of heterostructured CuO/CuWO₄ nanowires and thin films. *J. Cryst. Growth* **480**, 78–84 (2017)
- [9] Dong, Y., Tian, B., Kempa, T. J. & Lieber, C. M. Coaxial Group III–Nitride Nanowire Photovoltaics. *Nano Lett.* **9**, 2183–2187 (2009)
- [10] Butanovs, E., Kuzmin, A., Zolotarjovs, A., Vlassov, S. & Polyakov, B. The role of Al₂O₃ interlayer in the synthesis of ZnS/Al₂O₃/MoS₂ core-shell nanowires. *J. Alloys Compd.* **918**, 165648 (2022)
- [11] Sun, Y., Sun, B., He, J. & Wang, C. Compositional and structural engineering of inorganic nanowires toward advanced properties and applications. *InfoMat* **1**, 496–524 (2019)
- [12] Polyakov, B. *et al.* Unexpected Epitaxial Growth of a Few WS₂ Layers on {1100} Facets of ZnO Nanowires. *J. Phys. Chem. C* **120**, 21451–21459 (2016)
- [13] Butanovs, E., Kuzmin, A., Butikova, J., Vlassov, S. & Polyakov, B. Synthesis and characterization of ZnO/ZnS/MoS₂ core-shell nanowires. *J. Cryst. Growth* **459**, 100–104 (2017)
- [14] Butanovs, E. *et al.* Fast-Response Single-Nanowire Photodetector Based on ZnO/WS₂ Core/Shell Heterostructures. *ACS Appl. Mater. Interfaces* **10**, 13869–13876 (2018)

- [15] Zhu, X. *et al.* Enhancing Performance of a GaAs/AlGaAs/GaAs Nanowire Photodetector Based on the Two-Dimensional Electron–Hole Tube Structure. *Nano Lett.* **20**, 2654–2659 (2020)
- [16] Pearton, S. J. *et al.* A review of Ga₂O₃ materials, processing, and devices. *Appl. Phys. Rev.* **5**, 011301 (2018)
- [17] Shi, J. *et al.* Wide Bandgap Oxide Semiconductors: from Materials Physics to Optoelectronic Devices. *Adv. Mater.* **33**, 2006230 (2021)
- [18] Green, A. J. *et al.* β -Gallium oxide power electronics. *APL Mater.* **10**, 029201 (2022)
- [19] Pearton, S. J., Ren, F., Tadjer, M. & Kim, J. Perspective: Ga₂O₃ for ultra-high power rectifiers and MOSFETS. *J. Appl. Phys.* **124**, 220901 (2018)
- [20] Kaur, D. & Kumar, M. A Strategic Review on Gallium Oxide Based Deep-Ultraviolet Photodetectors: Recent Progress and Future Prospects. *Adv. Opt. Mater.* **9**, 2002160 (2021)
- [21] Wang, S. *et al.* In situ synthesis of monoclinic β -Ga₂O₃ nanowires on flexible substrate and solar-blind photodetector. *J. Alloys Compd.* **787**, 133–139 (2019)
- [22] Xie, C. *et al.* Catalyst-Free Vapor–Solid Deposition Growth of β -Ga₂O₃ Nanowires for DUV Photodetector and Image Sensor Application. *Adv. Opt. Mater.* **7**, 1901257 (2019)
- [23] Zhu, X. *et al.* Ga₂O₃–MXene Nanowire Networks with Enhanced Responsivity for Deep-UV Photodetection. *ACS Appl. Nano Mater.* (2023)
doi:10.1021/acsanm.2c05050
- [24] Sivakumar, C. *et al.* High-Quality Single-Crystalline β -Ga₂O₃ Nanowires: Synthesis to Nonvolatile Memory Applications. *Nanomaterials* **11**, 2013 (2021)
- [25] Krawczyk, M. *et al.* Morphology of Ga₂O₃ Nanowires and Their Sensitivity to Volatile Organic Compounds. *Nanomaterials* **11**, 456 (2021)

- [26] Afzal, A. β -Ga₂O₃ nanowires and thin films for metal oxide semiconductor gas sensors: Sensing mechanisms and performance enhancement strategies. *J. Mater.* **5**, 542–557 (2019)
- [27] Teherani, F. H. *et al.* A review of the growth, doping, and applications of β -Ga₂O₃ thin films. *Proc. SPIE 10533, Oxide-based Mater. Devices IX, 105330R* (2018)
- [28] Khartsev, S., Nordell, N., Hammar, M., Purans, J. & Hallén, A. High-Quality Si-Doped β -Ga₂O₃ Films on Sapphire Fabricated by Pulsed Laser Deposition. *Phys. Status Solidi Basic Res.* **258**, 2–6 (2021)
- [29] Kyrtos, A., Matsubara, M. & Bellotti, E. On the feasibility of p-type Ga₂O₃. *Appl. Phys. Lett.* **112**, 032108 (2018)
- [30] Li, J.-S. *et al.* Deposition of sputtered NiO as a p-type layer for heterojunction diodes with Ga₂O₃. *J. Vac. Sci. Technol. A* **41**, 013405 (2023)
- [31] Butanovs, E., Dipane, L., Zolotarjovs, A., Vlassov, S. & Polyakov, B. Preparation of functional Ga₂S₃ and Ga₂Se₃ shells around Ga₂O₃ nanowires via sulfurization or selenization. *Opt. Mater. (Amst).* **131**, 112675 (2022)
- [32] Chikoidze, E. *et al.* p-Type Ultrawide-Band-Gap Spinel ZnGa₂O₄ : New Perspectives for Energy Electronics. *Cryst. Growth Des.* **20**, 2535–2546 (2020)
- [33] Chi, Z. *et al.* Bipolar self-doping in ultra-wide bandgap spinel ZnGa₂O₄. *Mater. Today Phys.* **20**, (2021)
- [34] Chen, M.-I., Singh, A. K., Chiang, J.-L., Horng, R.-H. & Wu, D.-S. Zinc Gallium Oxide—A Review from Synthesis to Applications. *Nanomaterials* **10**, 2208 (2020)
- [35] Jang, Y. *et al.* Thin film transistors based on ultra-wide bandgap spinel ZnGa₂O₄. *Appl. Phys. Lett.* **116**, 202104 (2020)
- [36] Wu, Y. *et al.* A strategy of high-sensitivity solar-blind photodetector for fabricating graphene surface modification ZnGa₂O₄/Ga₂O₃ core-shell structure nanowire

- networks. *Ceram. Int.* (2023) doi:10.1016/j.ceramint.2023.02.196
- [37] Lou, Z., Li, L. & Shen, G. High-performance rigid and flexible ultraviolet photodetectors with single-crystalline ZnGa₂O₄ nanowires. *Nano Res.* **8**, 2162–2169 (2015)
- [38] Yu, Z. *et al.* Synthesis of ZnGa₂O₄ nanowires with β -Ga₂O₃ templates and its photoluminescence performance. *Mater. Lett.* **63**, 37–40 (2009)
- [39] Chang, K.-W. & Wu, J.-J. Formation of Well-Aligned ZnGa₂O₄ Nanowires from Ga₂O₃/ZnO Core–Shell Nanowires via a Ga₂O₃/ZnGa₂O₄ Epitaxial Relationship. *J. Phys. Chem. B.* **109**, **28**, 13572 (2005)
- [40] Promdet, P., Carmalt, C. J. & Parkin, I. P. Preparation and photocatalytic activity of ZnGa₂O₄ - β -Ga₂O₃ thin films. *Mater. Adv.* (2023) doi:10.1039/D2MA01016J
- [41] Wang, Z. *et al.* Tuning the selectivity toward CO evolution in the photocatalytic conversion of CO₂ with H₂O through the modification of Ag-loaded Ga₂O₃ with a ZnGa₂O₄ layer. *Catal. Sci. Technol.* **6**, 1025–1032 (2016)
- [42] Jin-Liang, Y., Yin-Nu, Z. & Chao, L. Formation of ZnGa₂O₄ films by multilayer deposition and subsequent thermal annealing. *Chin. Phys. B.* **23**, **4**, 048105 (2014)
- [43] Nedzinskas, R. *et al.* Temperature-dependent modulated reflectance of InAs/InGaAs/GaAs quantum dots-in-a-well infrared photodetectors. *J. Appl. Phys.* **117**, 144304 (2015)
- [44] Jangir, R. *et al.* Correlation between surface modification and photoluminescence properties of β -Ga₂O₃ nanostructures. *AIP Adv.* **6**, 035120 (2016)
- [45] Auer, E. *et al.* Ultrafast VLS growth of epitaxial β -Ga₂O₃ nanowires. *Nanotechnology* **20**, 434017 (2009)
- [46] Cheng, L.-C. *et al.* Effect of Defects on the Properties of ZnGa₂O₄ Thin-Film Transistors. *ACS Appl. Electron. Mater.* **1**, 253–259 (2019)

- [47] Harwig, T., Kellendonk, F. & Slappendel, S. The ultraviolet luminescence of β -gallium sesquioxide. *J. Phys. Chem. Solids* **39**, 675–680 (1978)
- [48] Jeong, I.-K., Park, H. L. & Mho, S. Two self-activated optical centers of blue emission in zinc gallate. *Solid State Commun.* **105**, 179–183 (1998)
- [49] Fan, H. J., Yang, Y. & Zacharias, M. ZnO-based ternary compound nanotubes and nanowires. *J. Mater. Chem.* **19**, 885–900 (2009)
- [50] Dolgonos, A., Mason, T. O. & Poeppelmeier, K. R. Direct optical band gap measurement in polycrystalline semiconductors: A critical look at the Tauc method. *J. Solid State Chem.* **240**, 43–48 (2016)
- [51] Zanatta, A. R. Revisiting the optical bandgap of semiconductors and the proposal of a unified methodology to its determination. *Sci. Rep.* **9**, 11225 (2019)